Laboratory Imaging of Satellites and Orbital Appearance Estimation

David Wellems
David Bowers
Applied Technology Associates, 1300 Britt St SE, Albuquerque NM, 87123-3353

ABSTRACT

For an increasingly cluttered space environment, having detailed pre-launch image information that can be used to predict and help interpret space object appearance is essential. Laboratory and extrapolated imagery provide important diagnostic information in the event of a satellite malfunction and assist in space object discrimination. Important discrimination factors include object optical cross-section and object spectrum. Understanding laboratory measurement limitations such as the dependence of unresolved cross section on source size and source coherence is critical in enabling these predictive capabilities. High resolution bi-directional reflectance functions (BRDFs) are used to extrapolate laboratory scale model imagery to space-like scenarios or determine the unresolved cross section. In these instances setups must reduce unwanted back ground light and mimic solar glint and diffuse earth shine at appropriate solar phase angles. Image extrapolation is performed in the spatial frequency domain and requires that the imager modulation transfer function (MTF) and source and sensor characteristics be understood.

1.0 Introduction

This paper discusses methods for obtaining image diagnostic data for subsequent on-orbit appearance estimates of pre-launch satellites or existing space objects. Prelaunch images of the actual object, in partially regulated lightning and model images in carefully controlled lighting and viewing geometries, would be the best approach for on-orbit appearance estimation. Model studies would help determine optimum viewing conditions or methods for glint reduction, or help interpret observational data or close-in imagery. Because space weathering alters appearance, some bi-directional reflectance distribution function (BRDF) data from the passive optical assembly (POSA) MIR experiments is presented in this document. The POSA samples, including paint, glass, coatings and metals, were exposed for 19 months in the 1996-1997 to the LEO space environment. Because we obtained these samples in 2004, possible earth resident weathering effects may have occurred. POSA spectral BRDF data for space weathered Kapton, thermal paints and aluminum is presented. Also, POSA data is been used to model space objects and estimate space object polarization.

Creating a model is the most challenging part of a study, but once constructed, model data can be obtained at corresponding solar phase angles and different object orientations. We do not know of any efforts using physical models to explain telescope observations or space object appearance. An ideal scale model would consist of satellite surface materials, and include articulating solar panels, and, if possible, simulate space weathering effects. Many satellites perform orientation and translation movements to orient antennas or align telescopes, and a gimballed model mount and moveable source would be needed for model illumination studies.

Conformal wrinkling of multi-layer insulation (MLI) material, or precise duplicate orientation of deployed solar panels or other specular surfaces for exact glint registration is not practicable or likely. Studies at different solar phase angles could determine whether overall reflective functions, BRDFs or optical cross sections could be used for describing the visual magnitude. Depending on the level of interest in an object's appearance, a good model and measurements would provide reference information and be of assistance in interpreting observations. Laboratory studies might help in determining rotation rates or rotation axis, size, shape, age, and material composition of a satellite or space debris. Emphasis would be placed on using materials that contribute most to the overall reflectance. Protective thermal or MLI blankets, thermal coatings, solar panels materials, and treated or untreated aluminum panels are materials that contribute significantly to object brightness.

A model imagery archive would include many illumination and viewing scenarios. Pre-launch images of an actual satellite are helpful for model construction, but incomplete because the satellite is not in its on-orbit configuration. Image documentation of cable harness and equipment placement may be important because of possible payload shifts. The satellite appearance based on pre-launch photos taken in diffuse room lighting conditions will differ markedly from the on-orbit appearance. Model studies are needed because the pre-launch satellite is in a controlled chamber or room, not easily maneuvered, the geometries are restricted by room size and other obstacles, the time available for imaging studies is small, company satellite engineers are finicky about personnel in proximity to the satellite, and there may be security and proprietary issues.

The system information inferred from image data after the external systems have been wrapped in protective MLI is limited, but useful. Pre-launch photos prior to MLI application would be useful. Satellite systems, such as fuel

tanks, reaction wheels, electrical cables, and communication equipment are wrapped in MLI protective materials, so that limited information would be obtained from close-in on-orbit inspections. Components not fully covered included thrusters, camera apertures, antenna and or MLI protected wiring harnesses, which may be imaged against reflective MLI backdrops. Glint mitigation methods such as using co/crossed linear or circular source and receiver polarizers, or using bandpass filters would be of interest. Measurement of laboratory satellites may help identify satellites and on-orbit status. For example, for near specular phase angles, if solar panel glint of certain magnitude was not observed, the satellite panels may not have deployed properly. Also, if a satellite was positioning so as to relay information, particular brightness variations might be observed.

Space weathering effects include oxidation, ultraviolet (UV) damage, surface contamination from propellants and outgassing, impact damage from dust and space debris. Kapton and Teflon MLIs are susceptible to oxidation effects in LEO. POSA-MIR data presented in this document shows that Kapton foil glints will be sharply reduced, though not altered spectrally, for those surfaces exposed to the on-orbit atomic oxygen particle stream. Surface erosion effects could be simulated using a scouring pad to abrade shiny metallic materials such as Kapton. Some POSA materials and coatings, though space weathered, retained specularity and would not be considered diffuse reflectors. Contamination due to rocket propellants, outgassing, venting of materials and waste water dumps have played a significant role in the degradation of thermal control surfaces and associated changes in optical reflectance [1]. Thermal cycling and UV may cause paints and MLI materials to flake or become brittle as on the Hubble Space Telescope [2]. Sample surface erosion of materials brought back from the Solar Maximum spacecraft at 500 km orbit showed 0.5 - 30.0 percent erosion. A Teflon surface was only moderately eroded [3]. Solar panels sustain numerous micro-debris impacts, and depending on satellite design, thermal stresses may warp panels effecting solar glint intensity.

Lack of knowledge of object size and mass are major sources of tracking errors of objects experiencing atmospheric drag. If better estimates of cross section could be achieved through understanding of optical models, information concerning the satellite's purpose or status could be obtained. Laboratory comparisons of optical cross section (OCS) and radar cross section (RCS) could prove useful for object identification or for improved estimates of the aerodynamic cross section. The Space Surveillance Network (SSN) radar provides RCS and orbital data from different radar sites. The RCS varies with radar wavelength depending on the object size, shape and materials. SSN optical telescopes are used for deep space and GEO objects which are not resolved. The European Space Agency's (ESA) 1 m telescope can detect +20 magnitude objects at GEO distances of 36,000 km [4]. The RCS detection limit varies with range, wavelength, orbit inclination and beam elevation. The SSN catalogue lists objects larger than 100 cm^2, which is about the UHF radar limit in LEO. For GEO distances, the minimum RCS is about 1 m^2. UHF radar cross sectional data are subject to many influences resulting in size estimates errors exceeding an order of magnitude [5]. MIT's 10 Ghz Haystack radar [6] can detect a -58 dBm^2 microwave reflecting object at a 1000 km range and is used to map LEO space debris with sizes less than 100 cm^2. The Haystack 10 GHz radar detects about a factor of 100 more objects than listed in SSN catalogue.

OCS and RCS comparisons of two LEO objects using the Experimental Test System (ETS) and Lincoln Laboratory's Haystack Radar were similar or widely different as described in [7]. Observed optical cross sections are inferred from visual magnitude data or laser returns. The observed OCS is typically the least well characterized parameter of the range equation [8] because of many uncertainties concerning the object. Radar's usefulness as a probe of the intrinsic properties of debris objects, such as composition, surface texture, and albedo, is limited [9].Laboratory spectral BRDF measurements of space weathered materials can be used to estimate object brightness or OCS of space debris.

The number of smaller orbital debris objects increases rapidly with decreasing size. Debris in 1-10 cm size range are too small to be tracked by US-SPACECOM[4] although NASA has used the Haystack/LRIR to sample statistically the LEO population at smaller sizes. Based on estimates derived from these radar observations, there are at least 130,000 orbital debris objects between 1 and 10 cm in diameter. From the time of the first launch until 1996, 59 shuttle windows had to be substituted due to impact craters; the largest crater ever revealed on a Shuttle window is a 1.2 cm diameter crater on STS-59, caused by a paint flake. Detailed analysis of the impacts on STS-73 can be found in [10].As of 1996, the Space Shuttle would suffer an average value of 1.1 crater/day of flight. Space debris is a growing problem. International cooperation will be needed to mitigate debris hazards or space will become unusable.

Laboratory experiments, even those that show hyperspectral signatures or active or passive cross sections may not be a good means of discrimination for certain objects, could prove useful. In this paper, model images, OCS and unresolved object spectral data for an HST model and a box satellite model are presented. Studies using diffuse illumination, as would occur from earth shine in a space based scenario, are of interest because the information content is highest for this type of illumination. Also, BRDF measurements of space weathered materials could help infer the brightness of particular debris types, such as fragment of embrittled MLI, paint flakes, solar cells, aluminum panels, and painted fuel tanks, some of which would not be in the SSN catalogue.

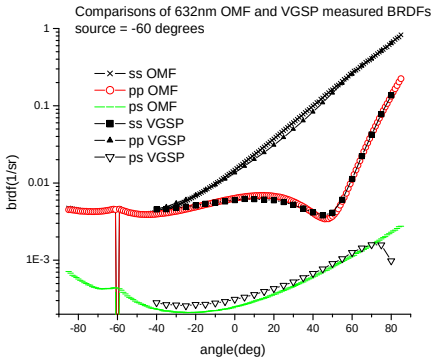

Figure 1. Krylon black BRDFs using OMF laser source and AFRL/VGSP incandescent lamp at 632 nm, source at -60 deg

Different numerical simulations such as TASAT and STK are available for predicting on-orbit appearance or pose, and may yield reasonable results depending on the object and illumination geometry. For instance, simple objects with diffuse gray or Lambertian appearances are generally modeled accurately in point source lighting conditions. For specular surface materials, such as solar panels with different layering, or satellites, which have a complex surface topology, numerical surface radiance predictions are problematic. The optical fidelity of numerical simulations is limited because these rely on BRDF data obtained at only a few wavelengths and spatial geometries. The BRDF model fit to the BRDF data may not be accurate. Simulations which treat the sun as point source instead of a disk, do not use BRDFs for multiple scatter, do not include space weathering effects, are often limited by lack of accurate spectral information, and usually do not include diffuse earth shine. Model data should be used to improve simulations.

2.0 BRDF Definition

Scientific literature describing an object's reflective brightness makes use of the term albedo or diffuse reflectance. The space debris community has adopted the convention of attributing space debris brightness to a spherical Lambertian scatterer with an albedo of .08 [7]. Typically for visual magnitude estimates, an interplay of often loosely determined and somewhat interrelated parameters including albedo or reflectance, size, orientation and solar phase function are used. Because the scattered intensity distributions for point source illuminated surfaces contain both directional and diffuse components, describing reflective brightness of an unresolved object in terms of albedo or reflectance may be confusing. If surfaces' broadband BRDFs could be used to determine brightness, a more meaningful and accurate description would result. If laboratory experiments demonstrated that an overall object BRDF or optical cross section with an appropriate phase angle dependence could be utilized, then this would be useful for understanding observations.

The scalar or unpolarized BRDF, $\varrho(r_i, r_r)$ of Eq. 1 relates incoming radiance Li coming from a solid angle $\delta\Omega_i$ to the surface radiance Lr observed along r_r. The vectors r_i and r_r are of unit magnitude and are referenced to the average surface normal, $\mathbf{z}$, and are centered on $\delta\Omega_i$ which is the incremental hemispherical solid angles or source solid angle. These vectors point outward from the surface.

$$dLr(r_r) = \varrho\ Li(r_i) r_i \cdot \mathbf{z} d\Omega_i \tag{1}$$

The unpolarized BRDF definition, which has units of sr^{-1} is given in [11]and $r_i \cdot \mathbf{z} = cos(\theta_i)$. Implicit in this definition is that the BRDF for a material does not vary across the source illumination or the observation region. The material BRDF should be independent of the material mounting, which ideally would be perfectly flat. BRDF measurements of rough or slightly rough surfaces are simpler than for very specular or shiny surfaces.

A measured BRDF should be independent of the source coherence or source angular size and region of interest (ROI). The maximum measurable BRDF, $BRDF_{max}$, which has units of $1/sr$ is determined by the angular diameter or the divergence of the source or $1/\Delta\Omega_i\ sr^{-1}$. Stated more simply, the angular divergence of the scatter or BRDF with units $1/sr$, must be smaller than $Rfl/\Delta\Omega_i$ for an accurate measurement. Here Rfl is the Fresnel smooth surface reflectance. A Lambertian or diffuse surface would be independent of view angle and have a BRDF value of $1./\pi$. If the surface is described as having an albedo, α, then the associated BRDF is α/π.

In the case of a sun source, the solid angle subtense is 6.7e-5. The maximum observable BRDF in sunshine from a metallic surface, with a Fresnel reflectance of $Rfl \sim 1$, would be approximately 15,000. In a laboratory study using a smooth gold, a $BRDF_{max}$ value of 19,700 was obtained using a broadband incandescent un-collimated source with

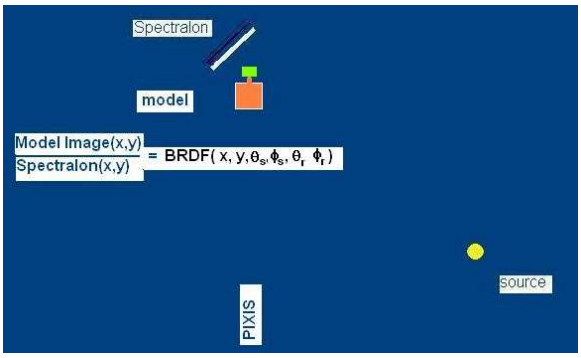

Figure 2. Panchromatic BRDF image definition

a .219" aperture, which was 30" from the sample. The predicted value of $BRDF_{max}$ was 24,000 for unity reflectance in this setup. Princeton instrument's Pixis camera was used for this result.

For very smooth or specular surfaces that can bend or wrinkle, such as solar cell films, MLI materials or solar cells arrays, BRDFs measurements become problematic. The BRDF may or may not depend on mounting, the source size and ROI sampling. For these types of materials, BRDF measurements are sensitive to many instrumentation and setup details. An averaged BRDF or cross section based on a larger BRDF image is more indicative of the dynamic range than a localized BRDF measurement. This is because individual solar cell tilts and many wrinkles contribute to intensity variations which are then averaged into the result.

The source coherence area for an incandescent lamp can be approximated by this expression [12]

$$A_{Src} \sim \lambda_a^2/\Delta\Omega_i \tag{2}$$

where $\Delta\Omega_i$ is the solid angle the source subtends and λ_a is the average wavelength. For an incandescent source 1" in diameter, placed .75 m from the surface and for a wavelength of .5 μm, the coherence area is $A \sim 5 * 10^{-5} m^2$ or the VGSP transverse coherence length is about 30 μm, which is smaller than the 50 μm coherence length of the sun at the earth's surface. The BRDF is a measure of the area of scattered field correlation. For a correct BRDF measurement, this area must be less than the area of source coherence.

To show that BRDFs can be independent of source coherence, consider results in Fig 1. This shows polarimetric BRDFs for commercial Krylon black spray painted aluminum. Measurements were made by the Optical Measurements Facility (OMF) using a highly coherent 632 nm HeNe laser for illumination and by Applied Technology Associates (ATA) using the visible grating spectral-polarimeter (VGSP), which has an incandescent source [13].The measurement agreement is excellent. The OMF laser-generated BRDF is smoothed because of speckle averaging. The s and p designations refer to the electric field vector alignment which is in or out of the plane of incidence.

3.0 BRDF Image Definitions

An ideal BRDF image is either a narrow band or panchromatic image showing the BRDF variation over an object for given view and source angles. Also, a diffuse BRDF image may be obtained by using a very wide angle or $\sim 2\pi$ sr uniform diffuse source. The BRDF image of an object is an intensity image that is normalized to a second intensity image of spectralon positioned at the object. Because spectralon has a known BRDF value, the BRDF image has units of $1/sr$ and is a measure of the surface radiant scatter. When the source and object inverse angular divergences (1/sr) are larger than the material BRDFs, the BRDF image can be used to predict the object intensity at much greater distances than for the setup geometry. Point source and diffuse BRDF images can be appropriately scaled and combined to simulate the surface radiance due to solar and earth shine. Corner cube arrays have very large BRDF values or small divergences in a monostatic configuration so that an incandescent source or bulb could not be used to determine the backscatter in a laboratory setting.

The setup for obtaining a BRDF image is shown in Fig 2. A dark smooth reflecting screen, such as smooth black plastic, rather than black cloth, can be used to deflect source light away from the model. Two images are needed to form the BRDF image where noise or dark currents in the images can be neglected or subtracted. A model image when divided by a reference image of spectralon forms the BRDF image. The BRDF image is a normalized or scaled intensity image which has units of $1/sr$. Depending on model scale feature sizes and the pixel region of interest (ROI), some BRDF averaging may occur. The BRDF of spectralon is approximately $1/\pi$ and may be used over a 250nm to 2500 nm range. The sum of co/crossed polarimetric spectralon BRDFs varying between .28 and .32 for zenith view angles ranging from -60 to 60 degrees for an incident angle of 0 degrees [14].Within these spectralon

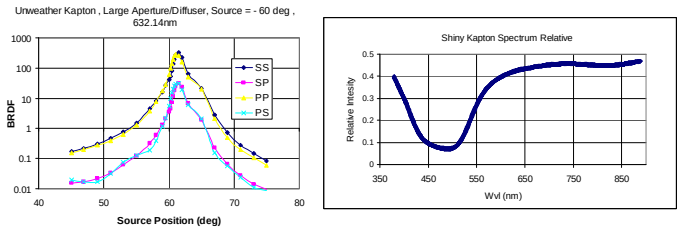

Figure 3. (lhs)632nm spatial, inc angle =-60 deg and (rhs) spectral polarimetric BRDFs for Unweathered Kapton, view angle = 0 deg, inc angle = -60 deg

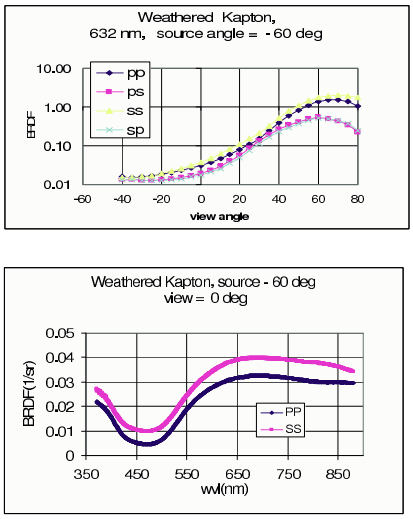

Figure 4. (lhs)632nm spatial, inc angle =-60 deg and (rhs) spectral polarimetric BRDFs for Weathered Kapton view angle = 0 deg, inc angle = -60 deg from MIR POSA-I samples

geometric constraints, the surface radiance of spectralon at location (x, y) is independent of view angle and is given by

$$S0(x, y, \lambda) = \int J(\theta_s, \phi_s, \lambda) cos(\theta_s) d\Omega \tag{3}$$

where θ_s, ϕ_s are the incident angles of the source ray where θ_s is the incident angle relative to the normal vector of spectralon, λ is the wavelength, and where the integral is over the angular subtense of the source with radiance, J and solid angle increment $d\Omega$. For a given wavelength, the BRDF image, which depends on view and source angles is

$$BRDF(nx, ny, \theta_s, \phi_s, \theta_v, \phi_v) = 1/\pi * ModelImage(nx, ny)/S0(nx, ny) \tag{4}$$

The $ModelImage(nx, ny)$ must be obtained with a linear scientific camera with a large bit depth such as the Princeton Pixis Si CCD camera.

$BRDF_{max}$ is an important quantity in scale model experiments. Because the source radiance of inexpensive broadband laboratory aperture controlled sources is less than the sun, apertures wider than angular diameter of the sun may be needed. If the BRDF image histogram is obtained using a laboratory source, and the surface glints satisfy $BRDF(x, y) << Rfl * BRDF_{max}$ where Rfl is the estimated specular or Frensel reflectance of the material for a known orientation, then the model BRDF image is representative of the BRDFs of the real object and the source size is not affecting the BRDF. The proximity of the source may result in improper shadowing of some model features, and if true, this should be shown to be unimportant to an overall result.

4.0 VGSP BRDF Data

BRDF data obtained with ATA/AFRL's VGSP is presented. Data from POSA-I samples and non-space weathered Kapton is presented. POSA-I was attached to the MIR Docking Module for an 18 month space exposure. Samples were returned to earth in 1997. A MIR sample of weathered RocketDyne CVS1147 Kapton and a non-weathered sample of Kapton are compared in Fig 4 and

Fig 3. For unweathered Kapton, the BRDF results depend on the ROI, mounting and the source diameter. LEO space weathering has reduced the peak Kapton BRDF intensity about a factor of 100. In the spectral domain, the

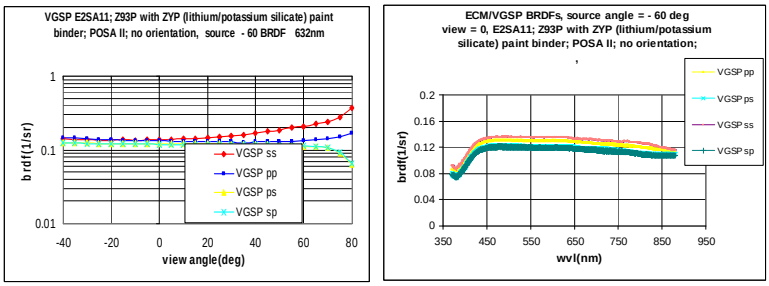

Figure 5. (left) 632nm Spatial polarimetric BRDFs and (rhs) source - 60, view angle = 0 or normal, incident angle = -60 deg, POSA-I Z-93 thermal coating

Kapton reflectance is smallest at blue wavelengths and approximately a factor of ten larger at red, NIR, and UV (375nm) wavelengths. The ps or sp values, when less than $1/2\pi$, are often associated with volume radiance. The reason for the large ps, sp or cross polarization components is due to wavelength dependent birefringence. The large Kapton sp and ps indicates that using non-orthogonal source and receiver polarizers would eliminate glint in a narrow band active illumination scenario. VGSP spectral results show that filters, which pass blue light, would reliably reduce glare.

Spectral polarimetric and 632nm spatial BRDFs are shown in Fig 5 for an inorganic thermal control coating, designated as Z-93 for the POSA-I samples. The paint is diffusely reflective at visible and NIR wavelengths, but less reflective in the UV range below 450nm. This coating may be an important space material because of its light weight and strength retention.

Spectral polarimetric and 632nm spatial BRDFs are shown in Fig 6 for space weathered aluminum of the POSA-I samples. This MIR sample retained considerable specularity in LEO orbit as evidenced by the large ss and pp BRDF peaks near 100 in the 632nm spatial scan. The presence of oscillations in the wavelength data and pink color suggests a layer a few hundred nanometers thick. The absence of large, cross polarizer components suggest there is little volume radiance associated with the sample. Based on this data, tumbling aluminum space debris from fragmentation or collisions would exhibit large changes in dynamic range.

5.0 Cross Section and BRDF image data

In this paper, the satellite OCS (m^2) is referenced to a 1 m^2 sample of spectralon and would be used to determine the brightness of an unresolved uniformly illuminated object at a large distance. Since spectralon is a Lambertian surface, the OCS (m^2) could also be converted to different units OCS(m^2/sr) by dividing OCS(m^2) by π as is sometimes seen in literature. The angular optical subtense of the object is $OCS(m^2)/(4.*\pi*R^2)$. The panchromatic passive broadband cross section has units of m^2 and is easily converted to apparent visual magnitude

$$V = -26.7 + 2.5log(4\pi^2 R^2/OCS(m^2)) \tag{5}$$

where R is observation distance. The extra factor of π allows for the BRDF of spectralon, which is used as a reference value. The sun has an apparent visual magnitude of -26.7, and the broadband cross section would ideally be obtained with a solar source simulator. A change in OCS by a factor of .01 or 100 results in a change of +/-5 for V.

The BRDF image may be accurate and specify the dynamic range in a scene. However, the cross section, as would be used at large distances, may be incorrect depending on smoothness of materials. To illustrate this, consider the solar glint from a smooth flat surface as would be evident when the camera is near the flat surface. As the camera distance from the surface increases, the solar disk occupies an increasing fraction of the flat. At some distance, the solar glint will occupy the entire flat. At this distance, the surface, as viewed from the camera location, has about the same angular extent as the source. Additional increase of the camera distance or increasing the aperture size will not impact the integrated BRDF image or the resulting cross section.

The cross section is derived by summing the BRDF image data obtained with a broadband source and is

$$OCS(\theta_s, \phi_s, \theta_v, \phi_v) = scl^2 * \frac{\sum BRDF(nx, ny, \theta_s, \phi_s, \theta_v, \phi_v)}{w^2/\pi} \tag{6}$$

where scl is the model scale factor, and w is numerical pixel width of the scaled 1 m^2 sample of spectralon, $BRDF(nx, ny)$ is the BRDF at the pixel. If the scale was 10:1, w pixels would need to span 10 cm in the image. For the laboratory measured cross section to be meaningful, small changes in geometry, such as decreasing the source aperture or increasing the camera distance should not impact the results. The VGSP BRDF data could also be used directly to the estimate OCS for a sample by using a size scaling factor and spectral averaging.

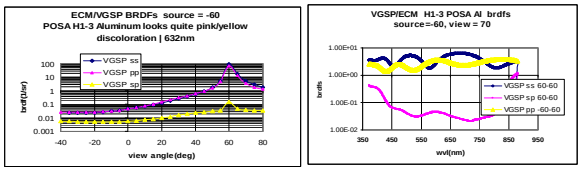

Figure 6. (top) 632nm Spatial polarimetric BRDFs and (bottom) source - 60, view angle = 70 POSA-I space weathered aluminum

6.0 Cross Section Measurements

We investigated models corresponding to the Hubble space telescope (HST) and a generic cube model consisting of a Kapton covered cube and a solar panel. The HST model was very similar in appearance to the actual system, but did not contain actual space materials. We suggest that if optical cross section data for an HST model with (Ag-FEP) MLI material had been obtained, reflective degradation due to space weathering of the insulation might have been monitored.

Results for the generic cube satellite are shown in Fig 7 consisting of EMCore solar cell film material and a kapton cube. A Labsphere source with a 2700 deg C color temperature was used. The small box satellite model is used to estimate cross section results for a 1 m^2 cube side, where the scaled solar panel size is approximately 1 meter high. The OCS for the cube model near the specular angle for the solar panel is variable depending on tiny angular tilts of panel. As the view and source distances increased, more of the panel began to glint, but a reliable convergent cross section for the glinting panel was not obtained because the OCS was so sensitive to the solar panel orientation. The source size was 1", so the angular source size decreases from .01 radians for the 100 " distance to .0025 radians at the 400" case. The associated maximum BRDFs with Rfl 1 would be $1.27 * 10^4$ and $2.03 * 10^5$, which would need to be multiplied by the solar cell film reflectance. It is not clear from these BRDF images that an infinite distance cross section for a specular geometry can be computed because of the large BRDFs near 4700. These results illustrate some issues with cross section measurements with very smooth surfaces at specular angles. Additional BRDF images need to be obtained at larger distances with an appropriate source size. The difficulty of making numerical models of these box satellite results is also apparent because of the complexity of the images. Also, for this model, in which the front Kapton surface was heavily wrinkled, the cross section was dominated by the Kapton when the solar panel was not glinting and the cross section variation was much smaller.

If an observed maximum physical model satellite cube cross section of approximately $100m^2$ from a 1 m^2 solar panel glint is used, this implies an apparent visual magnitude of + 10 and a non-glint kapton cube magnitude of approximately + 15 for GEO conditions. ESA's 1 m telescope observations of GEO objects showed the bulk of correlated objects in the + 10 to + 15 range [4] near the midnight anti-solar point.

Fig 8 shows the BRDF image and histogram of the HST model. The largest BRDF values of Fig 8 are associated with reflections from the telescope cylinder and the largest BRDF is approximately 35. The associated panchromotic cross section when scaled is 60 m^2. The apparent visual magnitude associated with this cross section for a 1000 km distance is 2.85. Glints from solar panels or flares would briefly increase the cross section.

7.0 Unresolved hyperspectral data

One approach for obtaining unresolved hyperspectral model is to use spectralon to collect scattered model light and then to measure the spectrum from spectralon. The ratio of the spectralon radiance spectrum to source spectrum generates a relative spectrum, which then could be weighted by the cross section to give a visual magnitude estimate. An advantage of using an imaging spectrometer to collect light from spectralon is that scattered light from the entire model is collected. A spectrometer with a narrow field of view collecting light might only collect light from a portion of a sample. Results for the HST and cube models are shown in Fig 9. The solar panel glint spectrum from the cube model is shown and is quite complex. This solar film spectrum changes with geometry because of different material layers in the solar cell and would be too difficult to model. The HST spectrum is relatively flat as is consistent with the silvery appearance of the telescope tube.

8.0 Image Extrapolation

The BRDF image is obtained by dividing the image obtained under small source illumination by an image of spectralon located at the same position under the same illumination conditions. The BRDF image at at given center wavelength, λ, is extrapolated using spatial frequency transfer functions, gain corrected and may be altered with additive noise to obtain a representative image for a particular optical system. The k-space extrapolated image is given by

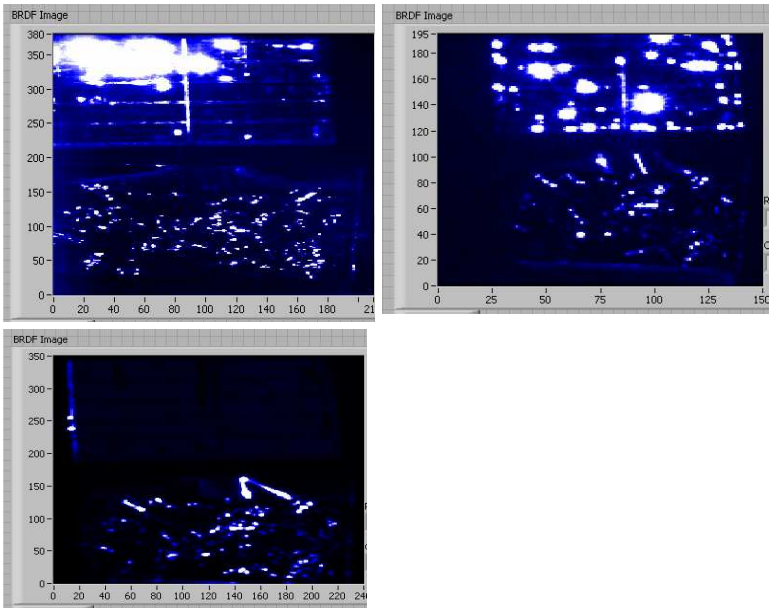

Figure 7. Panchromatic BRDF images with cross sections for Generic Cube Satellite, (a)110 m^2, max BRDF=4700, (b) 43 m^2, max BRDF=4700 and (c) 2.9m^2, max BRDF =189

$$Image(k_x, k_y, \lambda) = MTF(k_x, k_y, \lambda) FFT[BRDF(x, y, \lambda))] \tag{7}$$

where the overall MTF is given by

$$MTF(k_x, k_y, \lambda) = sinc(k_x * p_w) * sinc(k_y * p_w) * (1 - sqrt((k_x^2 + k_y^2))/k_{cut}) \tag{8}$$

This k-space image is Fourier transformed and is multiplied by the responsivity or camera gain map and by the solar irradiance to obtain either a broadband or narrow band image. An atmospheric MTF could also be included.

$$Image(x, y, \lambda) = Source * gain(x, y) * FFT[Image(k_x, k_y, \lambda)] \tag{9}$$

Fig 10 shows Pixis camera model BRDF images taken at a scaled distance of 158m, which was then extrapolated to 1.58km. The gain and source irradiance were not included. Note the loss of detail on the relay antenna. Because of the Pixis's large pixels, the MTF is dominated by pixels rather than the lens so that the image appears pixelated. A BRDF scale on the right side of each image is shown. This simple example illustrates the type of image that might be obtained from a fly-by space camera having large pixels.

9.0 Conclusion

We have presented a simple, but important, technique for generating BRDF images. If the maximum image BRDFs are less than Rfl/Δ, or the inverse source solid angle scaled by the estimated Fresnel reflectance of a glinting surface, the image can be used to compute an unresolved cross sections of a LEO or GEO space object. Laboratory OCS data may help interpret observational data. The model optical cross sections or apparent visual magnitudes were not inconsistent with observation of objects in GEO or reported HST magnitudes. However, the box satellite solar panel glints were quite variable depending on small, but uncontrollable, changes in panel orientation. For the HST model, the reflectance spectrum away from solar panel glints, was dominated by the telescope tube, and the HST OCS was 60 m^2. Image dynamic range can be inferred from the BRDF histograms, and this is important for sensor specifications. Strong glints from unweathered Kapton will mask detail for close-in images obtained with an 8-bit camera system. Because of birefringence, non-orthogonal alignment of source and receiver polarizers would‘ reduce Kapton glare. Also, blue filters will also reduce Kapton glare. Spectral polarimetric BRDF data for MIR-POSA samples was presented. Strong Kapton erosion effects were observed. Less erosion of bare aluminum samples and some POSA paints retained specularity or large BRDF values at specular angles. Unresolved hyperspectral data for each model was presented. For the HST, the spectrum was primarily determined by strong reflections from the telescope tube. Also, we presented an extrapolation methodology for predicting close-in satellite appearances in different imaging systems at different distances.

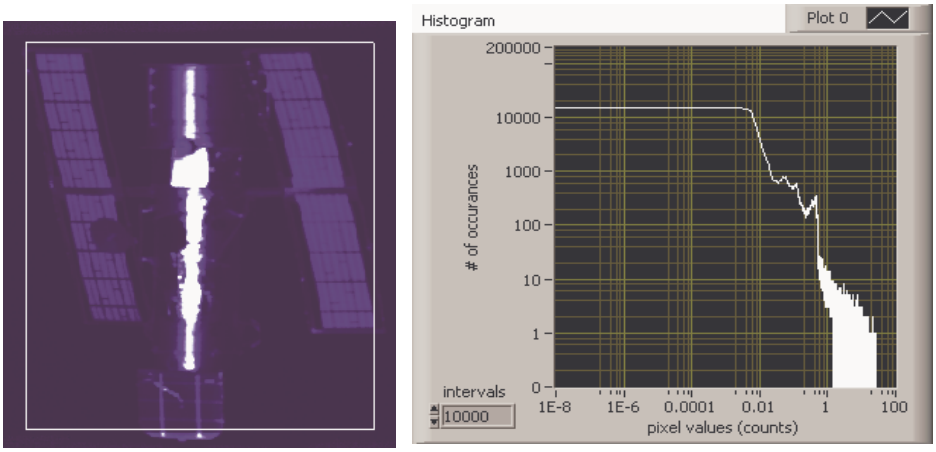

Figure 8. Panchromatic BRDF images of the HST Model and BRDF histogram

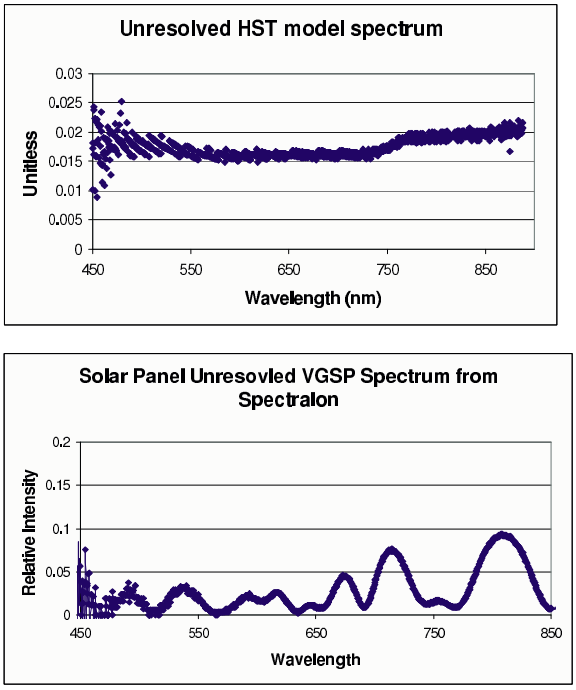

Figure 9. HST Model and Cube Solar Panel Model relative spectra

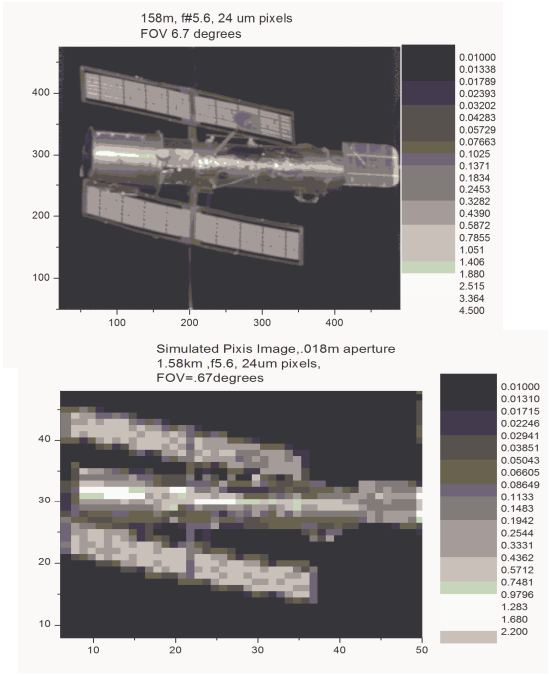

Figure 10. HST close-in and extrapolated BRDF images

REFERENCES

1. M. Hasegawa, H. Babel, " Estimation of the End-of-Life Optical Properties of Z-93 Thermal Control Coating for the Space Station Freedom", AIAA-92-2168-CP,1992
2. K. Groh, J. Dever, A. Snyder, et. al " Solar Effects on Tensile and Optical Properites of Hubble Space Telescope Silver-Teflon Insulation", NASA/TM -2006-214336
3. N.John Stevens," Methods for Estimating Atomic Oxygen Surface Erosion in Space Environments", *American Institute of Aeornautics and Astronautics, Engineering Notes*, Vol. 27, No 1, Jan-Feb, 1990
4. T. Schildknecht, R.Musci, M.Ploner,G.Beutler, W.Flury, J. Kuusela, J. de Leon Cruz, L. de Fatima Dominguez Palmero , " Optical observations of space debris in GEO and in highly eccentric orbits", *Advances in Space Research*, 34(2004) 901-911
5. Nicholas L. Johnson, Daivd J. Nauer, "Orbital Debris Detection: Techniques and Issues", AIAA/NASA/DOD Orbital Debris Conference, AIAA 90-1330
6. J. Beusch, I. Kupiec, MIT Lincoln Lab," NASA Debris Environment Characterization with the Haystack Radar", AAIAA 90-1346
7. D.M.Gibson, E.C.Pearce,M.S.Blythe,P.J.Trujillo,"Orbital Debris Characterization:ETS Staring Survey", SPIE Vol 1951, Space Debris Detection and Mitigation(1993)
8. G.Lukesh,S.Chandler,D. Voelz," Analysis of Satellite Laser Optical Cross Sections from the Active Imaging TestBed",Optics in Atmospheric Propagation and Adaptive Systems IV, Proceeding of SPIE Vol. 4538 (2002)
9. J. L. Africano, E. G. Stansberyb and P. W. Kervin, "The optical orbital debris measurement program at NASA and AMOS",*Advances in Space Research* Volume 34, Issue 5, 2004, Pages 892-900 Space Debris
10. Bernard R. and Christiansen E.: 1995, 'STS–73 Meteoroid/Orbital Debris Impact Damage Assesment Report', NASA JSC Report, JSC 27323, 15 Dec 1995.
11. K. E. Torrance and E. M. Sparrow, "Theory of Off-Specular Reflection from Roughened Surfaces", *Journal of the Optical Society of America*, **57**, No. 9, 1967.
12. L. Mandel and E. Wolf, "Optical coherence and quantum optics" Cambridge University Press, 1995, pg 153, 236.
13. J.A.Boger, S.D. Stokes, D.L.Bowers, B.R.Ratliff, M.P.Fetrow, " An error evaluation template for the use with imaging spectro-polarimeters", Proc. SPIE vol 5158, August 2003
14. C.L.Betty,A.K.Fung,J.Irons," The Measured Polarized Bidirectional Reflectance Distribution Function of a Spectralon Calibration Target" J.; Geoscience and Remote Sensing Symposium, 1996. IGARSS '96. 'Remote Sensing for a Sustainable Future.', International Volume 4, 27-31 May 1996 Page(s):2183 - 2185 vol.4 Digital Object Identifier 10.1109/IGARSS.1996.516929